# Highly Efficient Photoacoustic Conversion by Facilitated Heat Transfer in Ultrathin Metal Film Sandwiched by Polymer Layers

*Taehwa Lee and L. Jay Guo**

**Photoacoustic (PA) conversion of metal film absorbers is known to be inefficient because of their low thermal expansion and high optical reflection, as compared to polymeric materials containing light absorbing fillers. Here, highly efficient PA conversion is demonstrated in metal films. By using a metal film absorber sandwiched by transparent polymer layers, PA conversion is significantly enhanced, which is even comparable to in the highest reported in the CNT-polymer composites. Such enhancement is accomplished by ultrathin metal film (10 nm) capable of facilitating heat transfer to the adjacent polymers having high thermal expansion coefficient. This thin metal layer also allows integration of a photonic resonance cavity, effectively compensating the potential absorption loss of the thin metal. This strategy allows for easy spatial PA signal patterns and high conversion efficiency, which not only can be implemented for deep tissue PA imaging of implants or tools, but also provides a guideline for designing photoacoustic transmitters and contrast agents.**

## 1. Introduction

Photoacoustic (PA) generation (light-to-sound conversion) has been implemented for a myriad of applications ranging from PA imaging[1,2] and PA spectroscopy[3,4] (characterization of materials by measuring the sound at different frequencies) to nondestructive evaluation and test (NDE/NDT).[5] For those applications, PA signals usually need to be high enough to achieve a high sensitivity. Also, higher PA amplitudes allow imaging of targets located deeper in a sound-attenuating medium. Generating high-amplitude PA signals involves increasing input optical energy or choosing materials with more efficient PA conversion. But the maximum allowable energy can be limited to a damage threshold of the material or safety limits of biomaterials (tissue damage threshold, 20 mJ $cm^{-2}$[6]). Therefore, there is a strong need to find a system that can increase the PA conversion efficiency.

PA conversion, particularly via the thermoelastic effect, depends on material properties such as thermal expansion coefficient ($\beta$) and light absorption coefficient ($\alpha$) (i.e., Photoacoustic pressure amplitude, $P = \Gamma(\beta)\alpha F$ where the Grüneisen parameter, $\Gamma$ is a function of $\beta$, and $F$ is the laser fluence).[2] Efficient PA materials should have both high thermal expansion and good light absorption. Among many materials, metal films (typically, hundreds of nanometers thick) have been widely used due to easy fabrication and decent light absorption (e.g., >50% light absorption for Cr 100 nm at 532 nm wavelength). However, the PA conversion of metals is considered to be inefficient because of their low thermal expansion. Alternatively, researchers have developed composite materials with both high thermal expansion and good light absorption,[7–11] which consist of light-absorbing fillers embedded in transparent mediums with high thermal expansion. Specifically, an early attempt to make such composites was to use carbon black mixed with polydimethylsiloxane (PDMS), which showed an order of magnitude high PA amplitude compared to a metal film.[7] Recently, besides carbon black, other carbon materials including CNTs,[8,9] rGO,[10] candle soot nanoparticles,[11] and nanofiber[12] have been utilized as light-absorbing fillers, showing improved PA conversion efficiency. In addition to the carbon-based broadband absorbers, a metal-based PDMS composite consisting of gold nanoparticles was developed, showing high PA conversion efficiency compared to aluminum thin film.[13] Beyond imaging and sensing applications, such highly efficient PA materials have allowed new applications, e.g., PA cavitation therapy capable of selectively removing biomaterials, cells or tissues.[14–17]

Although the composite materials are proven to be promising, they have several disadvantages. For example, the composites require arduous preparation processes (e.g., high temperature CVD growth of CNT forest[8]). Also, the carbon fillers are easily agglomerated while mixing with polymers, thereby requiring surface functionalization of the fillers.[9] Moreover, for solution-processed composites, it is difficult to control the thickness of the films, especially if the composites contain a high concentration of fillers and thus become highly viscous.[8,18] Even though main contribution to efficient PA conversion is believed to be

Dr. T. Lee,[+] Prof. L. J. Guo
Department of Mechanical Engineering
University of Michigan
Ann Arbor, Michigan 48109, USA
E-mail: guo@umich.edu
Prof. L. J. Guo
Department of Electrical Engineering
and Computer Science
University of Michigan
Ann Arbor, Michigan 48109, USA

[+]Present address: Department of Radiology, Molecular Imaging Program at Stanford, Stanford University, School of Medicine, CA 94305, USA

DOI: 10.1002/adom.201600421

rapid heat transfer from light-absorbing fillers to the adjacent materials,[8,14] their complex morphologies make it difficult to theoretically analyze the composites and to fully understand the physics behind efficient PA generation in the composites.

In this work, we present a highly efficient PA conversion in a simple structure of a thin metal film sandwiched by transparent polymer layers. The metal film-polymer stack shows significant enhancement in PA conversion, as compared to a control sample made of metal film alone. Such increase is accomplished by two physical considerations: (1) using thinner metal layers (but less absorptive) that can facilitate heat transfer to the surrounding polymers and (2) by compensating light absorption loss with an optical resonance cavity. The facilitated heat transfer is experimentally confirmed by measuring PA signals for metal films of different thicknesses. This study could allow better understanding of PA generation in other composite structures, providing a useful design guideline. As a demonstration, the metal film-based composite is used for PA generation from spatial patterns, which could be useful for PA marking or PA imaging of medical tools and implants located deep inside the body.

## 2. Result and Discussion

### 2.1. Metal Film-Polymer Composite for High Efficient Photoacoustic Generation

#### *2.1.1. Structure of Metal Film-Polymer Composite*

The structure of proposed metal-based photoacoustic (PA) transmitter is illustrated in **Figure 1**a, which consists of a thin Cr layer (10 nm) sandwiched by two PDMS layers (top and bottom) built on a glass substrate. When a laser beam is irradiated from the glass side, the Cr layer absorbs incident pulsed laser beam (6 ns duration, 532 nm wavelength) and then converts the absorbed optical energy into heat energy. A portion of the heat energy is immediately transferred to the surrounding PDMS layers. The metal absorber is chosen to be as thin as possible so as to facilitate heat transfer to the surrounding PDMS layers having high thermal expansion coefficient. More efficient heat dissipation to the surroundings can result from reduced heat capacity ($C$) by using thinner metal absorbers ($C = \rho C_P V = \rho C_P A_s d$, where $\rho$, $C_P$, $V$, $A_s$, and $d$ are the mass density, specific heat capacity, volume ( $=A_s d$), surface area, and metal thickness, respectively). However, decreasing Cr layer thickness can reduce light absorption while increasing light transmission. To address this issue, a thin Al layer (50 nm) is deposited on top of the top PDMS layer as an optical reflector reflecting the transmitted visible light back to the Cr layer. Beyond simple reflector, the Al layer together with the Cr layer constitutes an optical resonance cavity, which significantly enhances the light absorption by the thin Cr layer. The proposed composite shows a drastic enhancement of PA amplitude (≈20 dB) compared to a bare Cr (100 nm) previously used by many researchers.

Figure 1b illustrates detailed PA generation process in the metal film-polymer composite. First, the excitation light is trapped in the optical resonance cavity and is strongly absorbed in the Cr layer. Light energy absorbed by Cr layer is transformed into heat, which is subsequently transferred to the adjacent PDMS layers. All the heated regions including the metal absorber and PDMS layers collectively contribute to output PA signals. Actually, the composite produces two oppositely propagating PA waves (backward and forward).[19] The backward wave is then reflected by the glass substrate, following the original forward wave. The reflected wave should pass through the thin Cr layer, which is acoustically transparent (because the acoustic wavelength is much larger than the thicknesses of the metal layers). Due to the path length difference, the reflected

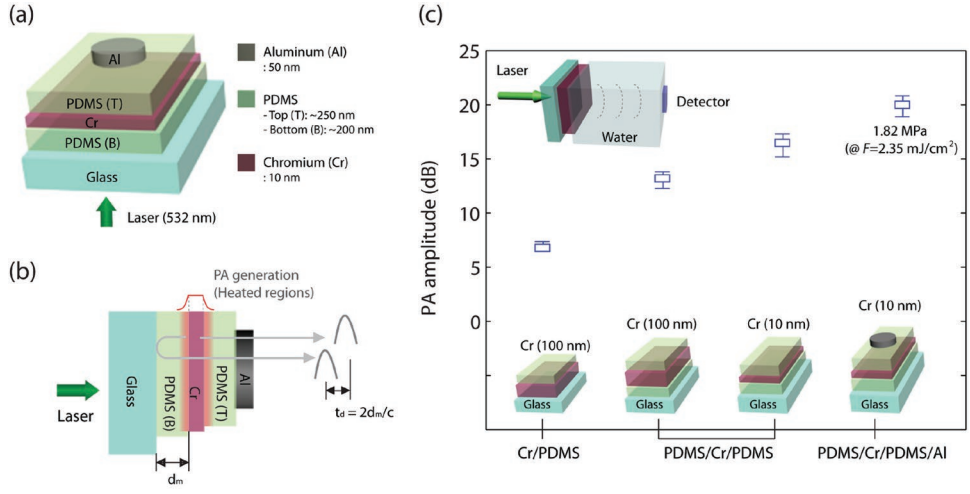


**Figure 1.** a) Metal film-based photoacoustic (PA) transmitter structure consisting of a Cr layer (10 nm) sandwiched by two thin PDMS layers. The Al layer (50 nm) serves as an optical reflector constituting an optical resonance cavity. Light is illuminated from the glass side. b) Illustration of detailed PA generation. Two oppositely-propagating PA pulses are produced in the heated regions. The two PA pulses have a delay time corresponding to twice the acoustic transit time across the bottom PDMS layer. c) PA signal amplitudes for different structures, normalized to the bare Cr (100 nm) on a glass substrate. The PA amplitude of the optimized structure is 1.82 MPa at a laser fluence of 2.35 mJ cm$^{-2}$.

photoacoustic wave has a delay time corresponding to twice the acoustic transit time across the bottom PDMS layer ($t_d = 2d_B/c$, where $t_d$,$d_B$, and $c$ are the time delay, the bottom PDMS thickness, and the sound speed of PDMS). Therefore, the bottom PDMS layer needs to be thin to avoid the broadening of output PA pulses that can reduce the output PA amplitude. The thin bottom PDMS layer is spin-coated by using diluted PDMS solution, and its thickness is measured to be ≈200 nm (see the Experimental Section). Thus, the time delay due to the bottom PDMS is only 0.4 ns, which is much shorter than the laser pulse duration (6 ns).

#### 2.1.2. Mechanism of Enhanced PA Conversion

A series of samples were fabricated, and the results were compared in Figure 1c. The PA signals are measured at laser fluence F = 2.35 mJ cm$^{-2}$. All PA signals are normalized to the peak PA amplitude of the thick bare Cr sample (100 nm) in contact of water. The first control sample consists of a thick Cr layer (100 nm) and a PDMS layer, which shows ≈6 dB increase in PA amplitude. Unlike the bare Cr directly contacted with a water layer, this bilayer heats up the adjacent PDMS that has higher thermal expansion, thus producing higher PA signals. This result is true, as long as PA generation in the water layer adjacent to the Cr film falls into thermoelastic regime, rather than nonlinear regime where the water layer can experiences phase change or explosive expansion for strong PA generation.[20] By inserting an additional PDMS layer between the Cr layer and glass substrate, the two sandwiched structures of different Cr layer thicknesses further increase PA amplitudes. The enhancement is achieved by preventing from heat loss to the glass substrate (which has negligible PA generation). In fact, when light absorbers are in direct contact of substrates, heat loss to the substrates is significant (analysis will follow). It is interesting to note that the thinner Cr layer (10 nm) gives stronger PA signal, even though the thinner Cr layer has lower light absorption. This result indicates that the facilitated heat transfer compensates the reduced light absorption. Lastly, adding an Al layer for the optical resonance shows a further improvement. The measured PA amplitude of the metal composite integrated to the optical cavity was 1.82 MPa (at a laser fluence of 2.35 mJ cm$^{-2}$), which is comparable to polymer composites (e.g., CNT-PDMS composite[8]).

The highly efficient PA conversion of the metal composite is achieved by both thermal and optical managements. However, we should emphasize that the efficient PA conversion is mainly originated from the improved heat transfer to the PDMS layers with high thermal expansion. In fact, by only perfecting light absorption, one cannot expect such significant improvement, showing the only twice enhancement. Thus, our approach is in sharp contrast to previous efforts to improve only light absorption for efficient PA generation.[18,21] Although PA generation for metal absorbers with different adjacent mediums has been explored elsewhere,[22,23] they used thick metal absorbers (or large particles) that are not effective in dissipating the heat to the adjacent mediums. And heat waste by the substrates was not a main focus. Moreover, by using the thin film-based coating, photoacoustic lens[8] can be readily fabricated on a variety of material support structures as there is no high temperature process involved in making the polymer–metal–polymer stack structures.

#### 2.1.3. Highly Efficient Metal Film-Polymer Composite for Potential Applications

The metal film-polymer composite structure could be applicable for various PA applications because of easy fabrication. For example, the metal film composite can be coated on a concave surface for a PA lens capable of producing high-amplitude pressure at focus, as the fabricated PA lenses with the multilayer coating are shown in **Figure 2**a. The PA lens fabrication is scalable such that the PA lens can be fabricated on different sizes of substrates (6, 15, 25 mm). PA waves produced by the metal film-based PA lens are focused to a spot (<100 μm) where their amplitudes are high enough to reproduce our previously reported results based on the CNT composite-coated PA lens.[16,17,24] Figure 2b shows microcavitation and liquid microjetting produced by the metal film-based PA lens. For microcavitation, PA wave was focused on the glass surface and created microbubbles (200 μm) in water. When PA wave was propagated from water and focused at the water/air interface, liquid jets were emerged from the interface and deposited on the glass substrate. Also, the metal-based PA generation coating could be applied to implants and medical tools, allowing PA guidance of such tools for precisely placing them, especially when they are located deep inside the body.[25,26] Moreover, the composite coating can be used to create spatial PA patterns, which can be used as PA markings containing useful information.[26] To demonstrate this concept, we fabricated a pattern (M logo) using standard photolithography, as shown in Figure 2c. Each region has different PA conversion efficiencies (i. glass/PDMS, ii. glass/PDMS/Cr/PDMS, iii. glass/PDMS/Cr/PDMS/Al). Figure 2d shows the PA image of the logo, demonstrating the easy patternability of the stack structure. Since the patterned structure is made of the region with efficient PA conversion, it can be located much deeper in a sound-attenuation medium, as compared to patterns with inefficient PA conversion.

### 2.2. Facilitated Heat Transfer to the Surrounding Polymers

#### 2.2.1. Dependence of Photoacoustic Amplitude on Metal Absorber Thickness and Surrounding Polymer Media

The facilitated heat transfer from thinner metal layers with lower thermal capacity to the surroundings is considered to be responsible for more efficient PA conversion. To confirm the dependence of PA conversion on the heat capacity of metal absorbers, heat capacity is changed by easily varying the absorber thickness for the bilayers and sandwiched structures. Besides the metal layer thickness, the material properties such as the specific heat capacity and mass density can change heat capacity, and thus the two metals of different thermal properties (Cr and Ti) were chosen for comparison. Also, to see the effect of the surrounding polymer layer,

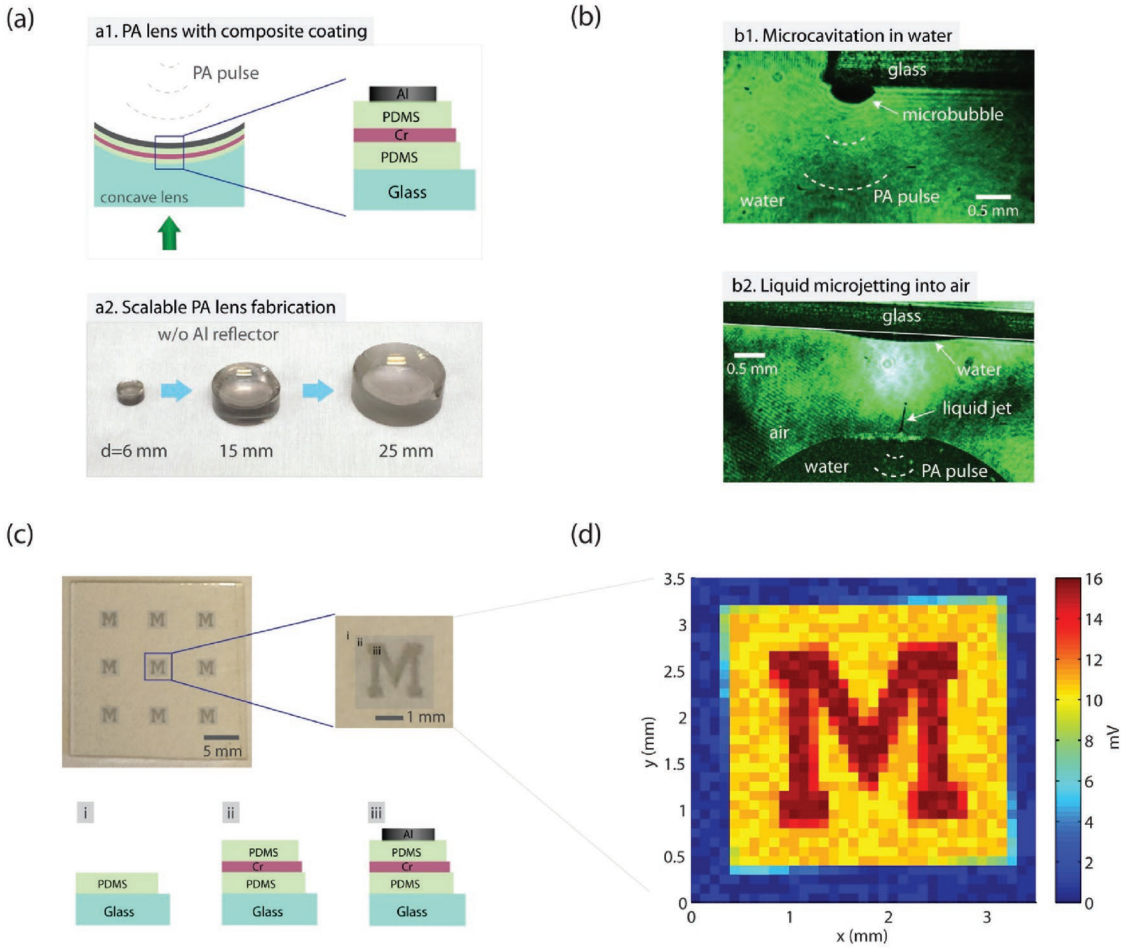


**Figure 2.** Metal film-polymer composite for applications. a) Schematics of PA lens consisting of the metal composite coated on plano concave lens (a1). The fabricated PA lenses with different diameters, d = 6, 15, and 25 mm before depositing the Al reflector (a2). b) Focused PA generation by the metal composite PA lens (d = 15 mm) for microcavitation in water (b1) and liquid microjetting into air (b2). The scale bar indicates 0.5 mm. c) Glass substrate with three different regions (i, ii, and iii), each with different PA conversion efficiencies. d) PA imaging of the patterned glass.

parylene was used for comparison with PDMS. The measured PA amplitudes for Cr and Ti samples without the Al reflector are shown in **Figure 3**a,b. For the Cr samples, the PA amplitude decreases with Cr layer thickness (10, 30, 50, and 70 nm) and then increases for 90 nm, while light absorption increases with Cr thickness for all the Cr samples [see Figure 3c]. The overall decrease in PA amplitude is likely due to the increased heat capacity of the thicker metal layers, and the increase for 90 nm is possibly because the increased light absorption compensates the increased heat capacity. For the Ti samples, the PA amplitude similarly decreases with Ti thickness except that the PA amplitude of 10 nm Ti sample is much lower than that of 30 nm one. This is because the light absorption of 10 nm Ti is significantly lower, compared to the others. By normalizing PA amplitude to light absorption and thus eliminating the effect of the change in light absorption, we can compare PA conversion of different metal thickness at the same light absorption. Clearly, the normalized PA amplitude decreases with the metal thickness, as shown in Figure 3e,f. Note that at the same thickness, the Ti samples better perform than the Cr sample (the optimized structure is based on Cr due to material robustness). This difference arises from lower mass density of Ti and thus lower heat capacity. These results indicate that lower heat capacity by either thinner metal layers or lower density indeed results in more efficient PA conversion. In addition, Figure 3a,b shows that PDMS coating layers provide stronger PA signal than parylene because of higher thermal expansion coefficient of PDMS.

### *2.2.2. Theoretical Analysis of Heat Transfer to the Adjacent Layers*

The enhanced PA conversion observed in the thin metal layers is theoretically investigated in terms of heat transfer. The heat energy in the metal absorber is dissipated into the surrounding mediums over relatively long time, but PA signals are just produced within laser excitation. Thus, it is reasonable to assume that heat energy during laser excitation is correlated to actual PA generation. We derived the heat energy in each layer using the Green's function method, based on an assumption of uniform temperature across the thin metal absorbers (see Supporting Information for detailed derivation). For the

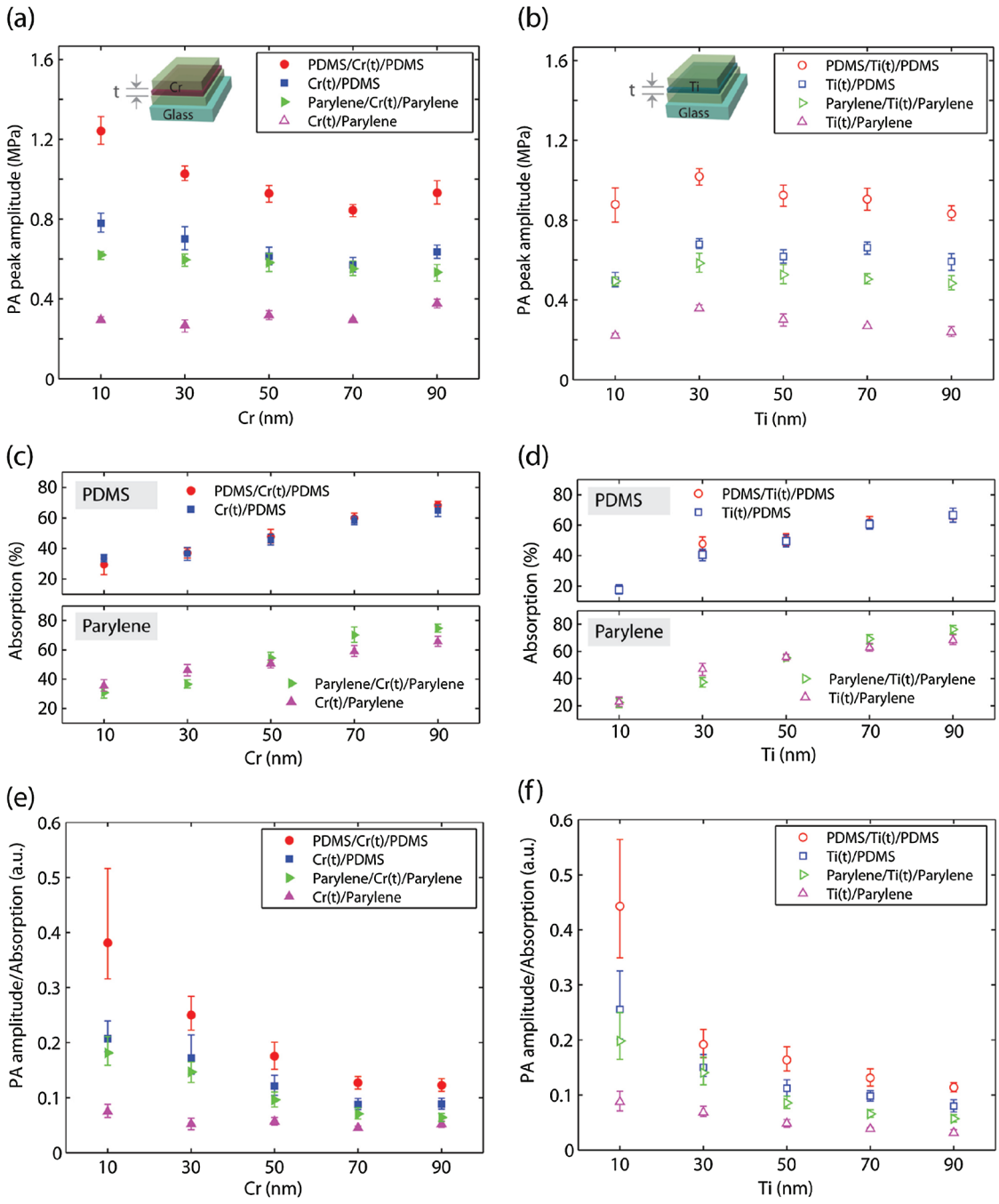


**Figure 3.** The measured photoacoustic (PA) amplitude as a function of metal layer thickness for a) Cr and b) Ti. The light absorption for c) Cr and d) Ti. The light absorption increases with the metal absorber thickness. The PA amplitude normalized to the light absorption for e) Cr and f) Ti. The normalized PA amplitude decreases with the metal absorber thickness.

sandwiched structure, the combined heat energy ($\gamma_s$) dissipated to the surrounding PDMS layers, normalized to the absorbed laser fluence ($A \cdot F$, where $A$ is the light absorption, and $F$ is the laser fluence), is represented by

$$\gamma_s = \frac{F_s}{A \cdot F} = \frac{2}{\frac{\rho_m C_{p,m} d_m}{\rho_s C_{p,s} l_{th,s}} + 2}, \text{and} \gamma_m + \gamma_s = 1 \quad (1)$$

where the subscripts m, s denote the metal and surrounding material, respectively, $d_m$ is the thickness of the metal layer, and $l_{th,\,s}$ is the heat penetration depth of the surrounding material $l_{th,s} = (1.269\alpha\tau)^{1/2}$, where $\alpha$ and $\tau$ are the thermal diffusivity and the laser pulse duration (full width at half maximum, FWHM). The heat energy calculated by the derived formula shows an excellent agreement with that obtained by the finite element method (see Supporting Information). Equation (1)

provides a very useful guideline, which states that the heat transfer is simply determined by the ratio of the heat capacities. Thus, heat transfer to the surroundings can be facilitated by either decreasing the heat capacity of the metal absorber or by increasing the heat capacity of the surrounding layer. Also, it is interesting to note that the heat capacity of the surrounding medium increases with the laser pulse duration, since the heat penetration depth depends on the laser pulse duration.

The calculated heat energy in each layer is shown in **Figure 4**a. The heat energy in the metal absorber ($\gamma_m$) increases with the metal absorber thickness ($d_m$), whereas the heat energy dissipated to the surrounding layers ($\gamma_s$) decreases regardless of the surrounding mediums (PDMS or parylene). These results are consistent with the previous approach of estimating the energy retained by the nanostructure based on the consideration of only surrounding medium's material properties, but provide better physical insights by considering the material properties of the light-absorbing medium. The heat energy in the surrounding layers becomes higher for Ti (due to its lower heat capacity than Cr) and PDMS (due to higher heat capacity than parylene). Specifically, for the structure (PDMS/Ti/PDMS), the thin Ti of 10 nm transfers almost 80% of heat energy to the PDMS layers, while for the thick Ti of 100 nm, 30% of heat energy is dissipated to the PDMS layers. Interestingly, the heat energy in the surrounding layer ($\gamma_s$) as a function of the metal thickness shows a similar trend as the normalized PA amplitudes (see Figure 3e,f). This trend can be explained by the fact that the output PA amplitude ($P$) is primarily determined by the PA amplitude produced in the surrounding materials with high thermal expansion ($P_s$), i.e., $P = P_m + P_s \cong P_s$. Here, $P_s$ can be represented by $P_s = A \cdot \Gamma \cdot (F/l) \cdot \gamma_s$,[27] where $A$, $\Gamma$, $F/l$, and $\gamma_s$ are the light absorption, the Grüneisen parameter, the energy volume density, and the heat energy in the surrounding layers, respectively. Therefore, the normalized output PA amplitude ($P/A$) can be expressed by $P/A \cong P_s/A = \Gamma \cdot (F/l) \cdot \gamma_s$. If the material properties ($\Gamma$) and energy volume density remain constant for different metal thicknesses, the normalized PA amplitude can be further simplified as $P/A \sim \gamma_s$. This relation indicates that the normalized PA amplitude is closely related to the transferred heat energy in the adjacent layers, explaining the similarity between the heat transfer to the surrounding layers and the normalized PA amplitude in the measurement.

#### 2.2.3. Effect of Glass Substrate on PA Generation

Figure 4b shows the calculated heat energy in each layer for various structures. For thick Cr layer (500 nm) in contact with water, the heat energy is mostly stored in the Cr layer (almost 90%). Thin metal absorbers are typically deposited on glass substrates in previous reports,[18,22] as seen for the structures (glass/Cr/water and glass/Cr/PDMS). It is noteworthy that the heat energy in the glass substrate is significantly high, because of high thermal diffusivity and thereby high heat capacity (see Equation (1)). In other word, considerable heat energy is just wasted to the substrate when absorbing materials are in direct contact with glass. The sandwiched structure built on glass substrate (PDMS/Cr/PDMS) can address this issue. However, adding the bottom PDMS layer increases the heat energy stored in the Cr layer, because the combined heat capacity of glass and the PDMS layer is higher than that of the two PDMS layers. By reducing the thickness of the Cr layer down to 10 nm, the thermal energy is effectively transferred into the surrounding PDMS layers (almost 70%). Thus, to make use of PDMS with high thermal expansion but with low heat capacity, it is very effective to use absorbers with much lower heat capacity for rapid heat transfer to the surroundings (e.g., low density nanometer-sized carbon fillers satisfies this requirement[8,11,12,27]).

### 2.3. Optical Resonance Cavity for Light Absorption

To increase light absorption in the thin metal layers, the optical resonance effect is used by employing the photonic Fabry–Parot cavity consisting of the Al reflector and the

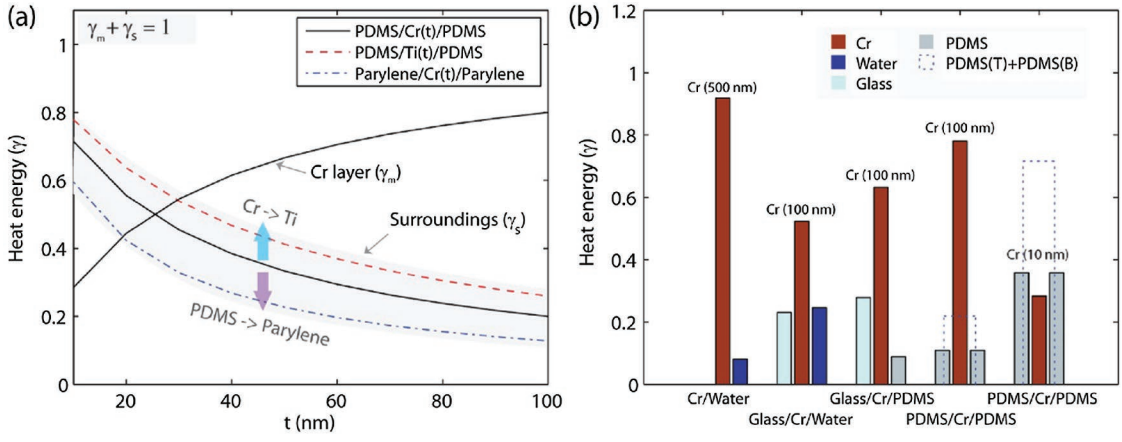


**Figure 4.** The calculated heat energy in each layer during laser excitation (pulse duration: 6 ns). a) The heat energy as a function of the metal thickness for the structure (PDMS/Cr/PDMS, solid line). The heat energy in Cr increase, while the combined heat energy in the PDMS layers decreases. The heat energy in the surrounding layers increases by replacing Cr with Ti (red dashed line), but decreases by replacing PDMS with parylene. b) The heat energy for different structures.

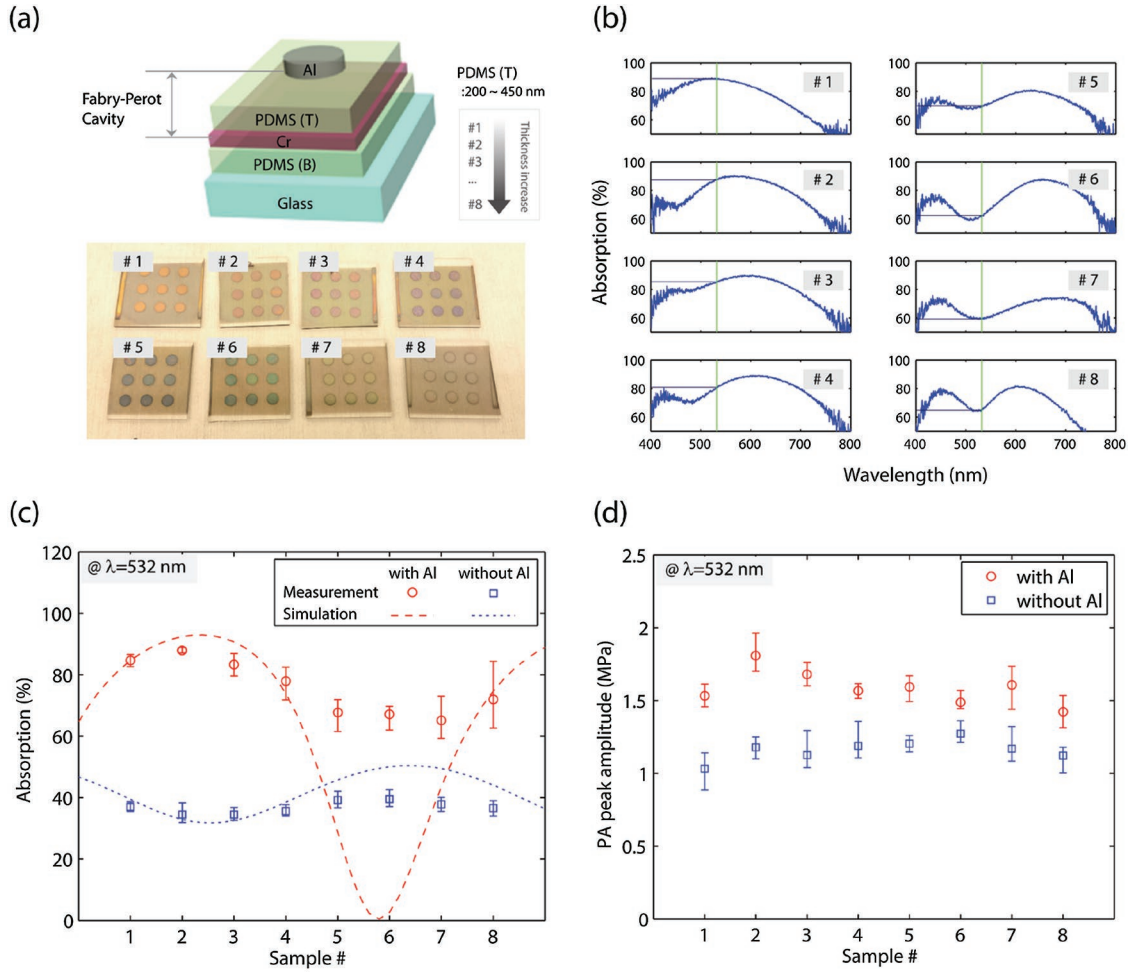


**Figure 5.** Light absorption by the optical resonance cavity. a) The structure with the Fabry–Perot cavity consisting of Cr and Al, spaced by the Top PDMS layer (i.e., cavity length). The reflective color is changed by increasing the cavity length (the length increases with the sample number). b) The measured light absorption spectrum for the samples. c) The measured light absorption at 532 nm for the structures with (circle symbol) and without (square symbol) the Al reflector. The calculated light absorption is also plotted for comparison. d) The measured PA amplitude at 532 nm for the structures with (circle symbol) and without (square symbol) the Al reflector.

Cr layer. The two metal layers are spaced by the top PDMS layer, whose thickness (i.e., cavity length) is properly chosen to allow constructive interference within the cavity. At the resonance condition, the light absorption in the Cr layer can be significantly increased up to 90%. **Figure 5**a shows that the resonance condition varies depending on the cavity length, as the reflective color changes with the top PDMS thickness (the thickness increases with the sample number). As the absorption spectrums of the samples are shown in Figure 5b, the absorption dip is red-shifted with increasing the cavity length. Also, the change in the cavity length modulates the light absorption at 532 nm wavelength (green vertical line), which is the laser source for exciting the PA generation. Figure 5c summarizes the measured light absorption at 532 nm for the samples with and without the Al reflector. Also, the calculated absorption (dashed lines) is plotted for comparison. With the Al reflector, the light absorption is increased, compared to the samples without the Al reflector. Regardless of the presence of the Al layer, the light absorption is modulated by the change of the cavity length. With the Al reflector, optical resonance occurs at a PDMS thickness of ≈200 nm, where propagation phase shift in the PDMS layer is completely cancelled by combined reflection phase shifts at the two metal interfaces. Interestingly, even without Al reflector, weak resonance effect was observed, because of the week light reflection at the interface between PDMS and air. However, without Al reflector, resonance condition is shifted by ≈0.87$\pi$, which corresponds to the reflection phase shift of the PDMS/Al interface. Note that without the reflector, the simulated light absorption shows a good agreement with the measured one. However, with the reflector, the simulated light absorption is deviated from the measured one, especially at the off-resonance condition. This deviation is possibly because the surface roughness of the spin-coated PDMS layer is high, thus leading to poor quality factor of the optical cavity (see Supporting Information for cavity roughness effect). However, the surface roughness effect could be practically beneficial for increasing the interfacial area and thus heat transfer across the interface. Also, even

if control of the cavity length fails, moderate light absorption would be ensured.

The measured PA amplitudes for the samples with and without the Al layer are shown in Figure 5d. By adding the Al reflector, the PA amplitude at 532 nm increases, showing a similar trend as the light absorption [Figure 5c]. However, the increase of the PA amplitude is smaller than the enhancement of the light absorption. Specifically, the PA amplitude at the resonance condition (sample #2) increases by less than two times, whereas the light absorption increases by more than two times. This nonlinear phenomenon could be related to temperature-dependent material properties.[28,29] The Grüneisen parameter of PDMS decrease with temperature,[23] meaning that higher light absorption causes lower PA conversion efficiency. We found similar phenomena by increasing laser pulse energy (see Supporting Information). Also, the Al layer could have a negative impact on PA propagation, which will be further investigated in a future study.

### 2.4. Photoacoustic Conversion Efficiency and its Comparison with Carbon Composites

The photoacoustic conversion efficiency can be calculated by

$$\eta = \frac{E_{aco}}{E_{opt}} = \frac{E_{aco}/A_s}{F} \tag{2}$$

where $E_{aco}$ is the acoustic energy, $E_{opt}$ is the laser pulse energy, and $F$ is the laser fluence ($E_{opt}/A_s$). By assuming the long pulse regime (i.e., Gaussian photoacoustic pulse has the same pulse duration as that of laser pulse ($\tau$, FWHM), $p(t) = P\exp(-2.77t^2/\tau^2)$), the acoustic energy per unit area can be represented by

$$E_{aco}/A_s = \frac{1}{\rho c}\int_{-\infty}^{\infty}\{p(t)\}^2\,dt = 0.75\frac{P^2\tau}{\rho c} \tag{3}$$

Thus, the photoacoustic conversion efficiency for the long pulse regime can be expressed by

$$\eta = 0.75\frac{P^2\tau}{\rho c F} \tag{4}$$

Since the PA amplitude ($P$) is proportional to the heat energy ($P \sim A\gamma F$), the conversion efficiency is linearly proportional to the laser fluence ($\eta \sim (A\gamma)^2 F$). As the PA conversion efficiency increases with the laser fluence, the measurement using higher laser fluence will result in higher PA conversion efficiency. To compare PA conversion efficiencies with other results using different laser energy, it will be more reasonable to use normalized conversion efficiency with respect to the incident laser energy, i.e., $\eta/F$.

The measured conversion efficiency of the optimized structure at 2.35 mJ cm$^{-2}$ is $0.42 \times 10^{-3}$, which corresponds to the normalized conversion efficiency $0.18 \times 10^{-3}$ mJ$^{-1}$ cm$^2$. By assuming perfect light absorption ($A = 1$) and ideal heat dissipation ($\gamma = 1$), the theoretical limit of the conversion efficiency at the same laser fluence is calculated to be $1.56 \times 10^{-3}$. The measured conversion efficiency is lower than the theoretical limit ($\eta_{th}$), because of light absorption loss ($A = 0.9$) and nonideal heat dissipation ($\gamma = 0.71$), i.e., $\eta/\eta_{th} < (A\gamma)^2 = 0.4$. The measured pressure amplitude of the sandwiched structure is smaller by 31% compared to the CNT-PDMS composites with 80% light absorption, which can be explained if the heat dissipation from CNTs to PDMS is very ideal ($\gamma \approx 1$), i.e., $(A\gamma)_{CNT\text{-}PDMS} \approx 0.8$. The energy conversion efficiency of the CNT composite is higher by $\eta/\eta_{CNT\text{-}PDMS} < (A\gamma)^2/(A\gamma)^2_{CNT\text{-}PDMS} = 0.63$. The carbon soot nanoparticle-PDMS (CSNPs-PDMS) was reported to be $4.41 \times 10^{-3}$ at a laser fluence of 3.57 mJ cm$^{-2}$, which corresponds to the normalized conversion efficiency of $1.24 \times 10^{-3}$ mJ$^{-1}$ cm$^2$, much higher than that of our sandwiched structure.[11] Such difference can be originated from difference in waveforms, as the waveform of the CSNPs-PDMS composite was reported to be broader than the laser pulse duration. In such case, comparing pressure amplitudes could be more reasonable. By assuming the linear relationship between laser fluence and pressure amplitude, the normalized pressure amplitude of the sandwiched structure (0.77 MPa mJ$^{-1}$ cm$^2$) is compared with that of CSNPs-PDMS (1.34 MPa mJ$^{-1}$ cm$^2$), showing about twice smaller amplitude. The better performance of CSNPs-PDMS can be understood by the ideal heat dissipation ($\gamma \approx 1$), i.e., $(A\gamma)_{CSNP\text{-}PDMS} \approx 0.95$, as compared to our sandwiched structure $(A\gamma) \approx 0.63$.

## 3. Conclusion and Discussion

We have demonstrated the highly efficient metal film-based composite photoacoustic (PA) transmitter based on the simple polymer-thin metal–polymer structure, which can be fabricated on a variety of substrates and easily scalable to large areas. In this structure, a very thin metal film (10 nm) is used as a light absorber such that the heat capacity of the metal absorber is significantly reduced, thus facilitating the heat transfer to the adjacent PDMS with high PA conversion efficiency. The sandwiched structure effectively prevents the heat loss to the glass substrate for PA generation. With the further integration of the optical resonance cavity, the light absorption in the thin metal layer is increased up to 90%. The PA amplitude is significantly higher than that of thick metal samples (one or two orders of magnitude higher), which is even comparable to that of the CNT-PDMS composite developed in our lab.[8] In fact, the physics that the new structure can significantly increase PA conversion efficiency closely mimics that of the carbon-based composites previously developed, which takes the advantage of good light absorption by the carbon nanomaterial and the high thermal expansion of elastomeric materials. In addition, the simple multilayer structure allows theoretical and experimental analysis of the heat transfer, ultimately providing a guideline for the design of contrast agents and PA transmitters. Also, the metal composite is free from the poor thickness control of the carbon composites. The composites based on mixing with light-absorbing fillers causes relatively thick films that could suffer from attenuation of high frequency PA signals. Lastly, the thin metal film-based composite could be useful for applications including PA imaging and scalable fabrication of PA transmitters.

## 4. Experimental Section

*Device Fabrication and Thickness Measurement*: The metals including Cr, Ti, and Al were deposited on glass substrates with or without coating layers by using a magneton sputter tool. PDMS solution diluted by hexane (PDMS:hexane = 1:20) was spin-coated for ultrathin PDMS layers of a few hundred nanometers (5000 rpm for 30 s). To vary the thickness of PDMS layers, spin acceleration was changed with 1000–4000 rpm $s^{-1}$. The thickness of prepared PDMS layer was measured by a stylus profilometer (Dektak 6M). The parylene layers were deposited by using a physical vapor deposition tool, producing a conformal coating on substrates.

*PA signal Generation and Measurement*: PA signals were generated by irradiating a nanosecond laser (pulse duration: 6 ns full with at half maximum, Surelite I-20, Continuum, Santa Clara, CA). The PA signals were measured by using a home-made broadband detector made of polyvinylidene difluoride (PVDF) with an active sensing area of 0.5 mm diameter and film thickness of 28 μm (estimated bandwidth: 40 MHz). The PA signals were displayed and recorded by using a digital oscilloscope (WaveSurfer 432, LeCroy, Chestnut Ridge, NY). For the characterization of the spatial PA pattern, the samples were moved by a motorized 3-axis translation stage with respect to fixed laser beam and the detector.

*Photonic Characterization*: The reflectance and transmission spectrums of the fabricated structures were measured by using a spectrometer (HR4000CF, Ocean Optics). Light absorption was calculated by subtracting the measured reflection ($R$) and transmission ($T$) (i.e., $1–R–T$).

*Simulation*: Light absorption of the multilayer structure was simulated by using a transfer matrix method. Heat transfer and PA generation were simulated by using a commercial software (the Courant number CFL < 0.05; COMSOL Multiphysics 4.3b).

## Supporting Information

Supporting Information is available from the Wiley Online Library or from the author.

## Acknowledgements

The authors would like to acknowledge the support from the National Science Foundation, Grant No. DBI-1256001.

Received: June 1, 2016
Revised: August 14, 2016
Published online: October 5, 2016

[1] X. D. Wang, Y. J. Pang, G. Ku, X. Y. Xie, G. Stoica, L. H. V. Wang, *Nat. Biotechnol.* **2003**, *21*, 803.
[2] M. H. Xu, L. H. V. Wang, *Rev. Sci. Instrum.* **2006**, *77*, 041101.
[3] D. W. Ball, *Spectroscopy* **2006**, *21*, 14.
[4] L. V. Wang, *Photoacoustic Imaging and Spectroscopy*, CRC Press, Boca Raton, FL, USA **2009**.
[5] D. M. McCann, M. C. Forde, *NDT&E Int.* **2001**, *34*, 71.
[6] K. Maslov, H. F. Zhang, S. Hu, L. V. Wang, *Opt. Lett.* **2008**, *33*, 929.
[7] T. Buma, M. Spisar, M. O'Donnell, *Appl. Phys. Lett.* **2001**, *79*, 548.
[8] H. W. Baac, J. G. Ok, H. J. Park, T. Ling, S. L. Chen, A. J. Hart, L. J. Guo, *Appl. Phys. Lett.* **2010**, *97*, 234104.
[9] R. J. Colchester, C. A. Mosse, D. S. Bhachu, J. C. Bear, C. J. Carmalt, I. P. Parkin, B. E. Treeby, I. Papakonstantinou, A. E. Desjardins, *Appl. Phys. Lett.* **2014**, *104*, 173502.
[10] S. H. Lee, M.-A. Park, J. J. Yoh, H. Song, E. Y. Jang, Y. H. Kim, S. Kang, Y. S. Yoon, *Appl. Phys. Lett.* **2012**, *101*, 241909.
[11] W.-Y. Chang, W. Huang, J. Kim, S. Li, X. Jiang, *Appl. Phys. Lett.* **2015**, *107*, 161903.
[12] B.-Y. Hsieh, J. Kim, J. Zhu, S. Li, X. Zhang, X. Jiang, *Appl. Phys. Lett.* **2015**, *106*, 021902.
[13] N. Wu, Y. Tian, X. Zou, V. Silva, A. Chery, X. Wang, *J. Opt. Soc. Am. B* **2012**, *29*, 2016.
[14] H. W. Baac, J. G. Ok, A. Maxwell, K. T. Lee, Y. C. Chen, A. J. Hart, Z. Xu, E. Yoon, L. J. Guo, *Sci. Rep.* **2012**, *2*, 989.
[15] H. W. Baac, J. Frampton, J. G. Ok, S. Takayama, L. J. Guo, *J. Biophotonics* **2013**, *6*, 905.
[16] H. W. Baac, T. Lee, L. J. Guo, *Biomed. Opt. Express* **2013**, *4*, 1442.
[17] T. Lee, H. W. Baac, J. G. Ok, H. S. Youn, L. J. Guo, *Phys. Rev. Appl.* **2014**, *2*, 024007.
[18] H. Yang, J.-S. Kim, S. Ashkenazi, M. O'Donnell, L. J. Guo, *Appl. Phys. Lett.* **2006**, *89*, 093901.
[19] T. Lee, Q. Li, L. J. Guo, *Sci. Rep.* **2016**, *6*, 21511.
[20] A. Prost, F. Poisson, E. Bossy, *Phys. Rev. B* **2015**, *92*, 115450.
[21] C. M. Chow, Y. Zhou, Y. Guo, T. B. Norris, X. Wang, C. X. Deng, J. Y. Ye, *J. Biomed. Opt.* **2011**, *16*, 017001.
[22] S. Kang, Y. Yoon, J. Kim, W. Kim, *Appl. Phys. Lett.* **2013**, *102*, 021908.
[23] Y.-S. Chen, W. Frey, S. Aglyamov, S. Emelianov, *Small* **2012**, *8*, 47.
[24] T. Lee, H. W. Baac, J. G. Ok, H. S. Youn, L. J. Guo, *Phys. Rev. Appl.* **2015**, *3*, 044007.
[25] J. L. Su, R. R. Bouchard, A. B. Karpiouk, J. D. Hazle, S. Y. Emelianov, *Biomed. Opt. Express* **2011**, *2*, 2243.
[26] T. Mitcham, K. Homan, W. Frey, Y.-S. Chen, S. Emelianov, J. Hazle, R. Bouchard, *J. Biomed. Opt.* **2013**, *18*, 56008.
[27] H. W. Baac, J. G. Ok, T. Lee, L. J. Guo, *Nanoscale* **2015**, *7*, 14460.
[28] I. G. Calasso, W. Craig, G. J. Diebold, *Phys. Rev. Lett.* **2001**, *86*, 3550.
[29] L. Wang, C. Zhang, L. V. Wang, *Phys. Rev. Lett.* **2014**, *113*, 174301.